Surface Instabilities and Magnetic Soft Matter

Christian Gollwitzer,
Experimentalphysik V, Universität Bayreuth, 95440 Bayreuth, Germany
Marina Krekhova*, Günter Lattermann†,
Makromolekulare Chemie I, Universität Bayreuth, 95440 Bayreuth, Germany
Ingo Rehberg and Reinhard Richter
Experimentalphysik V, Universität Bayreuth, 95440 Bayreuth, Germany

March 6, 2009

We report on the formation of surface instabilities in a layer of thermoreversible ferrogel when exposed to a vertical magnetic field. Both static and time dependent magnetic fields are employed. Under variations of temperature, the viscoelastic properties of our soft magnetic matter can be tuned. Stress relaxation experiments unveil a stretched exponential scaling of the shear modulus, with an exponent of $\beta = 1/3$. The resulting magnetic threshold for the formation of Rosensweig-cusps is measured for different temperatures, and compared with theoretical predictions by Bohlius *et. al.* in *J. Phys.: Condens. Matter.*, 2006, **18**, 2671–2684.

1 Introduction

Ferrofluids have found widespread applications in rotary seals, loud speakers, or medicine [1, 2]. They are a colloidal dispersion of magnetic nano particles in a carrier fluid like water or kerosene [3]. Due to their superparamagnetic behaviour, they can be controlled by externally applied magnetic fields.

The same is true for ferrogels [4–7], with the difference that here the magnetic nano particles are embedded in an elastic (polymer) matrix. This is handy for many upcoming applications, such as soft actuators, magnetic valves, magnetoelastic mobile robots [8], artificial muscles [9] or magnetic controlled drug delivery [10–13]. Most of the applications are based on the continuous *deformation* of ferrogel bodies in gradient fields [14] or in homogeneous fields [15, 16]. Another promising effect, which so far has not been exploited, is the drastic shape transition of ferrogels in the succession of the Rosensweig instability. If a threshold of the magnetic induction is surpassed, the flat reference state of the ferrogel is predicted to develop surface protuberances, pointing in the direction of the vertically oriented field. The critical induction B_c is derived by means of a linear stability analysis in Ref. [17]. It depends on the surface tension σ, the mass density ρ, the gravity g_0, and on the elastic shear modulus G of the gel according to

$$B_c^2 = 2\frac{\mu_0\mu_r(\mu_r+1)}{(\mu_r-1)}(\sqrt{\sigma\rho g_0}+G), \qquad (1)$$

where μ_0 is the vacuum permeability and μ_r is the relative permeability of the ferrogel. In comparison to the Rosensweig instability in ferrofluids ($G = 0$) [18] the threshold B_c is enhanced by the elasticity due to an increase of the surface stiffness. In contrast, the critical wavelength is independent of the elastic modulus of the gel and is described by the capillary wavelength

$$k_c = \sqrt{\frac{\rho g_0}{\sigma}}\,, \qquad (2)$$

*present address: Makromolekulare Chemie II, Universität Bayreuth, 95440 Bayreuth, Germany
†present address: Grüner Baum 32, 95448 Bayreuth

familiar from ferrofluids [18]. Like in the case of ferrofluids, neither the critical field nor the critical wavelength depend on the viscosity. Note that, in contrast to ferrogels, for the instability of a ferrofluid layer covered with a thin elastic film, it was predicted, that k_c decays drastically with increasing elasticity [19].

More recently, the authors of Ref. [17] derived the final pattern which forms in ferrogels [20]. These results are limited to patterns of small amplitude and were obtained via a minimisation of the energy density, similarly to the method used for ferrofluids [21, 22]. For ferrofluids, the energy density comprises hydrostatic, magnetic and surface terms. To account for the elastic deformations in ferrogels, an energy contribution as given in [23] is added. The Rosensweig instability in standard ferrofluids is associated with a transcritical bifurcation and exhibits a hysteresis [21, 24]. In ferrogels, this hysteresis is expected to shrink with increasing shear modulus [20].

The Rosensweig instability in ferrofluids has been studied in many experiments; see e.g. Refs. [18, 25–31]. However, its counterpart in ferrogels is still awaiting measurements. The reason for this void is that up to now mostly covalent cross linked polymer gels [5, 7, 32] have been synthesised. This process results usually in rather "hard" gels. Due to their high elasticity and the saturation of the magnetisation, one can not excite surface instabilities in these gels even for very high magnetic field strength. Only recently *soft ferrogels* have been created [6] which take advantage of thermoreversible, i.e. physically crosslinked gelators. Contrary to chemically crosslinked, irreversible ferrogels, their elasticity can be controlled by a thermoreversible sol-gel transition. In the following we investigate the Rosensweig instability in such a thermoreversible ferrogel.

2 Material and Methods

2.1 Synthesis

We prepared a thermoreversible ferrogel by swelling 5 wt.% of a gelator in an oil-based ferrofluid containing 30 wt.% of magnetite particles. The carrier liquid for the preparation of the ferrofluid was paraffin oil (Finavestan A50B from Total Deutschland GmbH) with a kinematic viscosity $\nu = 13.6\,\mathrm{mm^2/s}$ at 20 °C and a molar mass of 280 g/mol (manufacturer information). The magnetite particles were prepared by co-precipitation and stabilised with oleic acid [6]. Transmission electron micrographs show, that the diameter of the particles is 8 ± 1 nm [33]. As a gelator we have utilised Kraton G 1726 from Kraton Polymers, Belgium, which is a mixture of 30 wt.% triblock copolymer and 70 wt.% of a diblock copolymer. The triblock copolymer is poly(styrene-b-(ethylene-co-butylene)-b-styrene) (SEBS) with a molar mass of $\bar{M}_W = 77\,700$ and a polydispersity index PDI = 1.01 [33]. The diblock copolymer (SEB) is exactly one half of the triblock. The size distribution has been established by means of size exclusion chromatography. For both the di- and triblock copolymer the styrene content amounts to 30 wt.% (manufacturer information). In comparison with the pure triblock copolymers used in earlier studies [33], the diblock acts here as a plasticiser and lowers the softening temperature to 25 °C, according to the falling ball method [6]. Both the ferrofluid and the ferrogel reveal no structure in optical micrographs, i.e. they are perfectly homogeneous down to a sub-micrometer scale. The ferrogel sample remains stable for 1½ year without any separation of the fluid phase from the gelator, i.e. without any syneresis. Likewise, we did not observe changes of the magnetic properties and the microstructure within this time.

2.2 Material properties

For the characterisation of the elastic properties we utilise a rheometer (MCR 301, Anton Paar) in cone-and-plate geometry. The cone has a diameter of 50 mm and a base angle of 1°. The rheometer is equipped with a Peltier thermostated temperature device (C-PTD 200/E). Figure 1 displays the result of oscillatory measurements of the shear modulus at 1 Hz for a deformation of $\gamma = 0.01$ versus the temperature. G' and G'', which denote the real and imag-

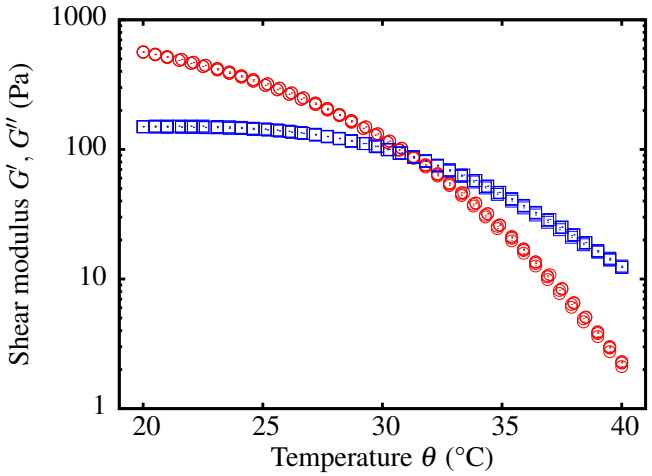

Figure 1: Storage modulus G' (red circles) and loss modulus G'' (blue squares) versus the temperature for the thermoreversible ferrogel.

inary part of the shear modulus, respectively, have a crossover around 31 °C. Above $\approx$ 45 °C, the sample becomes liquid.

To measure the magnetisation curve of the ferrogel, we produce a sphere by casting 1.0 ml of the liquefied gel into a hollow aluminium mold at 55 °C. For details see Ref. [16]. The magnetisation of the spherical sample was then measured by means of a fluxmetric magnetometer (Lake shore, model 480) at $\theta = 20$ °C. Figure 2 shows this data. The sample is superparamagnetic with an initial susceptibility of $\chi_0 = 0.82$. This data has been fitted with the model of Ivanov [34], assuming a gamma distribution of the particle diameters. We use this model as well to extrapolate $M(H)$ for all sample temperatures, by evaluating the fit with a different θ, while all other parameters are held constant. As an example, the dashed line gives the extrapolation for the maximal applied temperature of $\theta = 38$ °C.

The density ρ of the ferrogel is measured by immersing the sphere in water with added salt. The salt establishes a vertical density gradient which keeps the ball floating in the middle of the container at half depth. With the help of a syringe, water has been sampled directly above and below the ball. The density of both samples is then measured by means of a vibrating tube density meter (DMA 4100, Anton Paar Co.).

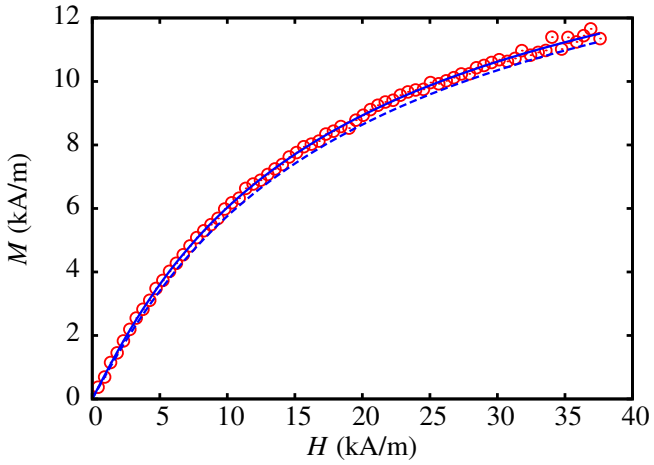

Figure 2: Magnetisation as a function of the applied magnetic induction for the thermoreversible ferrogel. The solid line represents a least squares approximation with the model put forward by Ivanov [34]. The best fit parameters for the gamma distribution are: exponent $a = 8.1 \pm 1.3$, mean diameter $x_0 \cdot (a+1) = 8.1 \pm 0.4$ nm, volume fraction $\phi = 3.9 \pm 0.09$ %. The core magnetisation has been held constant at $M_F = 446$ kA/m. The dashed line indicates the prediction for $\theta = 38$ °C with the above parameters.

From the mean of both values follows the density of the ball to be $\rho = 1085 \pm 1\,\mathrm{kg/m^3}$.
More cumbersome is an estimate for the surface tension σ. As a rough estimate, we measure the surface tension of the paraffin based ferrofluid the gel was created from with a ring-tensiometer (LAUDA TE 2). We get $\sigma_{\mathrm{FF}} = 28.7\,\mathrm{mN/m}$ for both the ferrofluid and also the underlying paraffin oil that was used as a carrier liquid for the ferrofluid. For obvious reasons, the tensiometer can not be directly applied to the ferrogel. Because the gelator is not surface active, it shall not have a significant influence on σ. We therefore use σ_{FF} in the subsequent calculations as the surface tension of the gel.

2.3 Setup for measurements of the normal field instability

Our experimental setup is shown in Fig. 3 (a). In the centre is a thermostated aluminium block of size (x,y,z)=(60,60,50) $\mathrm{mm^3}$. A cylindrical bore of 50 mm and a depth of 25 mm serves as a vessel for the ferrogel. A bore with the same diameter, but a depth of 23 mm penetrates the block from the lower side, in this way leaving a bottom plate with a thickness of 2 mm (cf. Fig. 3 a). Utilising thermal grease, the vessel is thermally connected to two Peltier elements, as shown in Fig. 3 (b). They are equipped with heat exchangers (1A cooling Co., type 1A-SL2), which are circulated by water from a closed cooling system (LAUDA RK20 KP). A thermo-resistor Pt100 serves to monitor the temperature of the vessel. The Peltier elements are powered by a DC-current source (EUROTEST Co., type LAB/SL 230/AI/LT) which is controlled via IEEE from the computer. By a proportional-integral method, the computer regulates the temperature of the vessel with a precision of 5 mK in the range of −35 °C to 110 °C. The vessel is covered from above by means of an aluminium plate with a thickness of 0.5 mm. This lid creates an isolation layer of air above the free surface of the ferrogel. We have chosen the small aspect ratio $\Gamma = h/d \approx 5$ of the container, because the amount of ferrogel was limited.
The vessel is fixed in the centre of a water

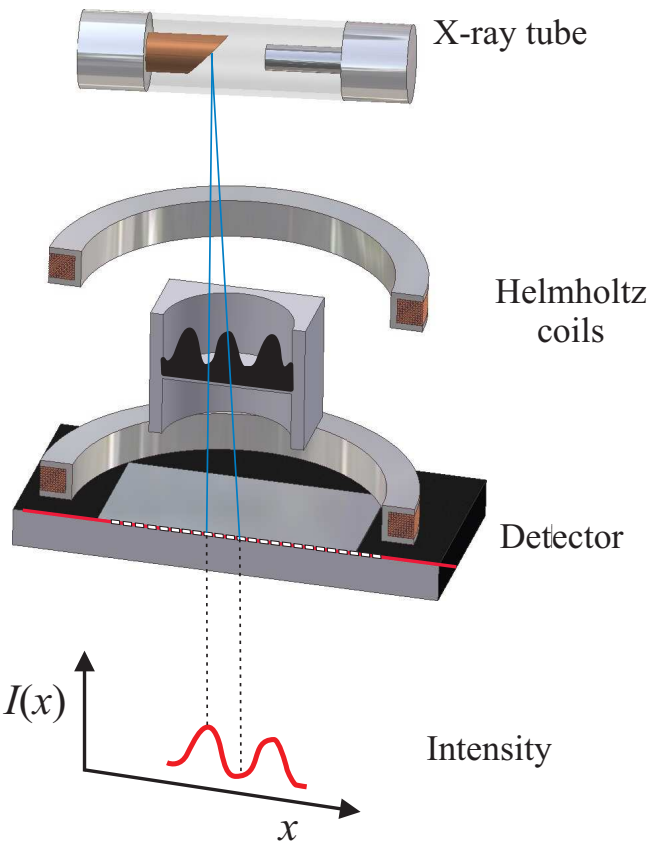

Figure 3: Experimental setup: (a) Scheme of the setup (not to scale); (b) photo of the temperature controlled container, filled with ferrogel.

cooled Helmholtz-pair-of coils (Oswald Magnettechnik Co.). An X-ray tube is mounted above the centre of the vessel at a distance of 1606 mm. We measure the attenuation of X-rays passing through the ferrogel layer in the vertical direction with a photodiode array detector, which has a lateral resolution of 0.4 mm. Rays which are passing through crests are more attenuated than those passing through valleys (cf. Fig 3 a). The full surface topography is then reconstructed from the radioscopic images. The dynamic range of the detector of 16 bits translates into a vertical resolution of 0.4 µm. This resolution is achieved only when averaging many frames (≈ 1000), because of a noisefloor with an RMS value of $h_{\mathrm{RMS}} = 20\,\mu\mathrm{m}$ for a single frame. The calibration of the absolute height is limited to ≈ 0.1 mm by the stability of the X-ray source and the mechanical positioning. For details see Refs. [30, 35].

Prior to each series of measurements, a batch of 12 ml of ferrogel is positioned in the empty vessel. This amount is molten by heating up the vessel to 90 °C, in this way creating a flat layer of ferrogel. Then the temperature is lowered to the desired value for the measurement and held constant.

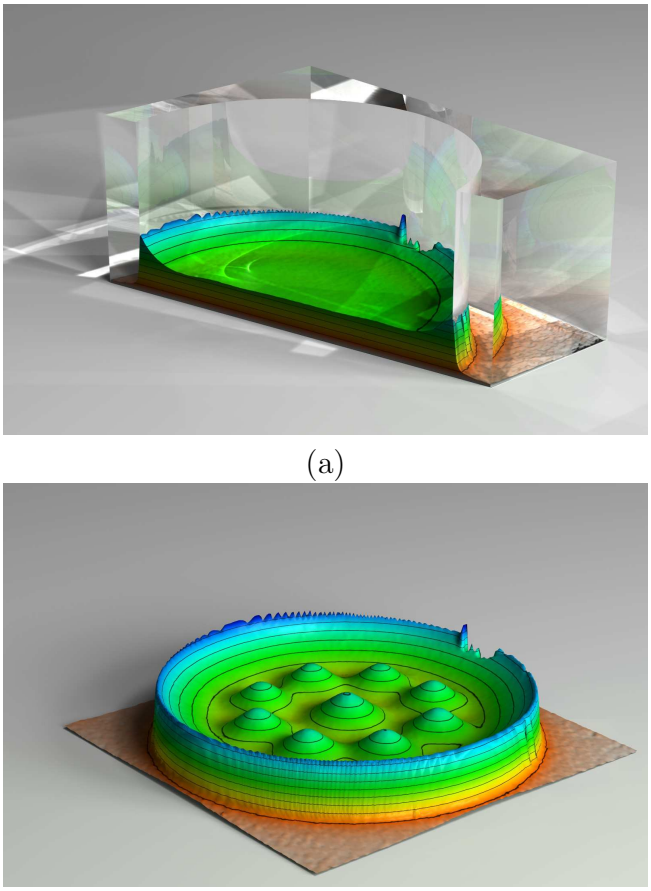

(a)

(b)

Figure 4: A Rosensweig pattern emerging in ferrogel, measured by radioscopy: (a) cross section for $B = 22.9$ mT; the transparent material illustrates the size of the aluminium container; (b) full profile for $B = 28.1$ mT. The black contour lines are indicating consecutive levels with a distance of 1 mm.

3 Results

3.1 Quasistatic Experiments

Figure 4 presents characteristic topographies of the ferrogel for subcritical (a) and supercritical inductions (b). Due to the step-like jump of the magnetisation at the container edge, a field gradient arises which attracts the ferrogel towards the container edge. Therefore a meniscus is formed. Chart (b) shows an example of the Rosensweig pattern. In the following, the height h of the central peak of the pattern serves as an order parameter and is estimated by fitting a paraboloid.

Figure 5 gives the variation of the order parameter for a slow increase (upward triangles) or decrease (downward triangles) of the magnetic induction for five different temperatures. In the interval from $B = 19$ mT to around 24 mT one

notices a monotonic decay. In this regime no spikes exist. However, due to the formation of a meniscus (cf. Fig. 4 a), the level of the material in the central part of the vessel, where h is estimated, decreases. For higher inductions, we observe a steep increase of h for all curves. It is this regime where the ferrogel spikes are emerging.

Whereas in laterally infinitely extended liquid layers the transcritical bifurcation gives a proper scaling of the order parameter [22], for small pools of ferrofluid, imperfections induced by the container edges obscure the analytical scaling law. In this case, only a numerical model is available [36, 37]. In lack of an analytical expression, we can not extrapolate the values for the critical induction B_c from a fit of $h(B)$. As an approximation for the threshold of the predicted discontinuous transition we determine the induction $B_{\mathrm{max.up}}$ where the amplitude $h(B)$ has its steepest inclination, i.e. $\partial h/\partial B = \max$. It is determined from a spline fit and listed in table 1 for all investigated temperatures. A lower bound for the threshold is given analogously from the data for decreasing magnetic induction. It is denoted by $B_{\mathrm{max.dn}}$. The hysteresis, defined by $B_{\mathrm{max.up}} - B_{\mathrm{max.dn}}$, is in the range of 2 mT at 30 °C and shrinks to a fraction of 1 mT at 38 °C, as shown in the zoom presented in Fig. 5 (b).

Next we check, whether the time for a measurement cycle in B has an influence on the evolution of the order parameter. In Fig. 6 we present the results for a measurement cycle of 2 h (red dashed line) and of 4 h (blue solid line) for a temperature of $\theta = 30\,^{\circ}\mathrm{C}$, which is the lowest temperature, at which the measurements discussed beforehand have been performed. One clearly sees that the hysteresis between the upward- and downward branch shrinks for longer cycle times. This variation is in the range of 1 mT.

For higher temperatures (and lower G) the influence of the cycle time becomes even less significant. Notwithstanding, the influence of the cycle time indicates, that we have different time scales in the ferrogel. These time scales will be studied next.

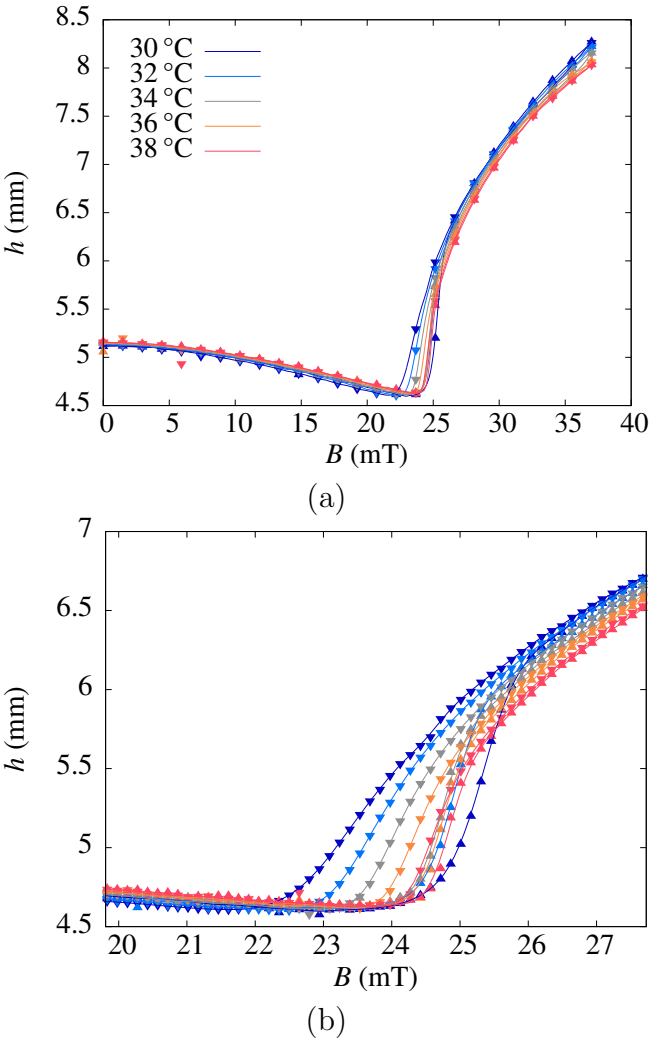

Figure 5: Height of the central peak for an increase (upward triangles) and decrease (downward triangles) of the magnetic induction. The colour encodes the temperature from 30 °C (blue) to 38 °C (red), as in the legend. (a) Full range. For clarity only every 10th data point is shown. The lines are splines to the full data set. The time for the measurement was 2 h. (b) Zoom of the hysteresis. All data points are shown.

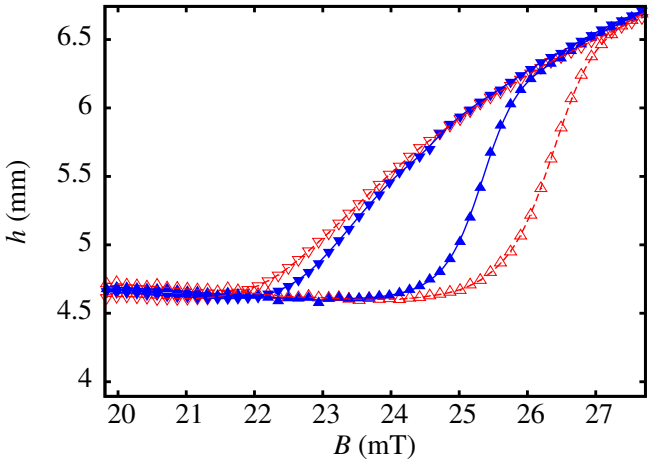

Figure 6: Height of the central peak for increasing induction (upward triangles) and for decreasing induction (downward triangles). The time between subsequent data points was doubled from 14.4 s (red dashed line) to 28.8 s (blue solid line). The time for a full cycle from 0 mT to 37 mT amounts to 2 h and 4 h, respectively.

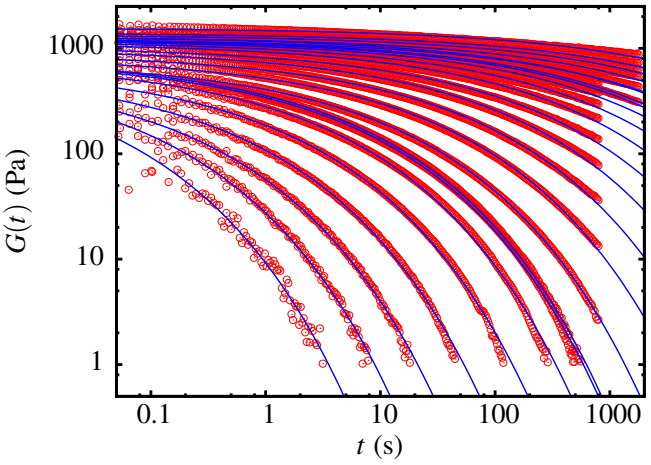

Figure 7: Time dependent shear modulus $G(t,\theta)$ after a jump in the deformation of $\gamma = 0.01$ for different temperatures of the ferrogel. The temperatures have been varied from $-10\,^{\circ}\mathrm{C}$ to $32\,^{\circ}\mathrm{C}$.

3.2 Dynamic Experiments

3.2.1 Stress Relaxation Experiment

In order to characterise the shear modulus G, we perform a stress relaxation experiment for a series of temperatures. We shear the sample by a deformation of $\gamma = 0.01$ and measure the relaxation of the stress τ while the deformation is held constant. Figure 7 displays the data points recorded for various temperatures of the sample. For a specific temperature, the restoring force decays drastically during one second, which means that in our experiment, the shear modulus $G = \tau/\gamma$ cannot be treated as constant.
Commonly, a stretched exponential function is used to describe the time dependent moduli of linear viscoelastic media [38–42]

$$G(t,\theta) = G_0(\theta)\exp\left(-\left(\frac{t}{t_0(\theta)}\right)^{\beta}\right). \qquad (3)$$

Here, the exponent β is restricted to the range $[0,1]$, with $\beta = 1$ for a simple exponential decay, and an increasingly broader distribution of relaxation times for smaller values of β. Moreover, this scaling law was recently observed in the stress relaxation of a triblock copolymer subject to an extensional strain [43], and consecutively explained in a model, which assumes that the copolymer reversibly splits into domains of different size [44]. These domains consist of a regular homogenous network of PS micelles which are interconnected by bridging chains of the middle block of the polymer. Also in our ferrogels, we observe glassy PS micelles arranged in clusters, which are interconnected by bridging chains of the ethylene-butylene middle block of the triblock copolymer gelator used. The size of these domains varies in the range from 60 to 120 nm [6, 33].
Next, we apply (3) to our relaxation data. The solid lines in Fig. 7 give approximations of $G(t,\theta)$ with (3) for different temperatures θ from $\theta = 32\,^{\circ}\mathrm{C}$ down to $-10\,^{\circ}\mathrm{C}$. This temperature range was determined by the resolution of our rheometer. All the fits use a common exponent β. The best value amounts to $\beta = 0.34 \pm 0.01$.
The characteristic relaxation time $t_0(\theta)$ of the ferrogel drops drastically with increasing temperature. It varies over six orders of magnitude, as shown in the Arrhenius plot Fig. 8. However, the dependence does not make up a straight line – therefore no simple Arrhenius behaviour with an activation energy can be inferred.
Thus we observe for all temperatures a stretched

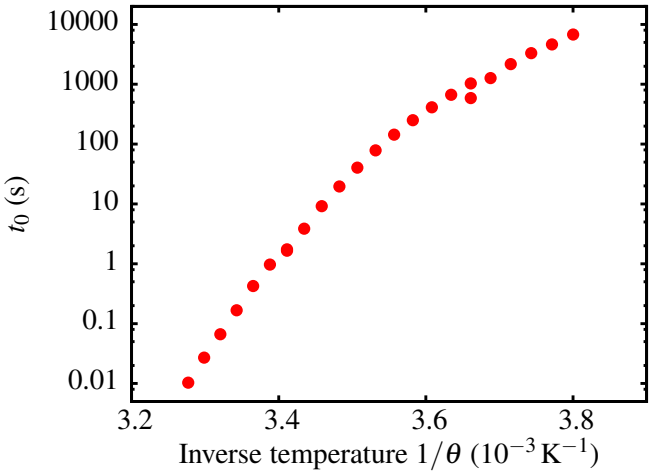

Figure 8: Arrhenius plot of the characteristic relaxation time. The data stem from fits of (3) to the measurements presented in Fig. 7.

exponential softening under load with a characteristic scaling exponent near 1/3 for all temperatures, while the characteristic relaxation time t_0 varies over six decades. These experimental findings are in agreement with the observation of domains [33] and the predicted scaling law based upon a reversible splitting of domains [44].

For $t \to \infty$, the time dependent shear modulus $G(t, \theta)$ approaches 0. This means, that we have a viscoelastic soft magnetic material, without any long term elasticity.

3.2.2 Periodic Driving Magnetically

In the effort of constraining G to some finite value, we are next selecting a specific time scale. We periodically drive the imposed magnetic induction according to

$$B(t) = B_0 + \Delta B \sin(2\pi f_D t). \qquad (4)$$

Here, B_0 denotes the bias value, $\Delta B = 1.6\,\mathrm{mT}$ the driving amplitude, and $f_D = 1\,\mathrm{Hz}$ the driving frequency of the induction imposed by the Helmholtz-pair-of-coils. For each sample temperature, we measure the surface response for 24 different values of B_0. For small B_0, the surface is oscillating with f_D around its meniscus-like shape, which becomes alternatingly more and less pronounced concave. Beyond a threshold, spikes appear which are oscillating with the amplitude Δh around a mean height $\bar{h}$ with the driving frequency. For the whole range of values, we observe a harmonic response which can be described by

$$h(t) = \bar{h} + \Delta h \sin(2\pi f_D t + \phi). \qquad (5)$$

In order to determine the quantities $\bar{h}$ and Δh, we measure the absorption of X-rays in the oscillating surface pattern by means of an X-ray movie. For each data point we record 2200 frames with a frame rate of 7.5 Hz. Each absorption picture n is transformed into a height profile $h_n(x, y)$. From the series of height profiles, we extract the desired quantities via the equations

$$\begin{aligned}
\bar{h}(x,y) &= \frac{1}{n}\sum_{1}^{n} h_n(x,y) \\
h_{\sin}(x,y) &= \sum_{1}^{n} \sin(2\pi f_D n\Delta t)\, h_n(x,y)\, W(n\Delta t) \\
h_{\cos}(x,y) &= \sum_{1}^{n} \cos(2\pi f_D n\Delta t)\, h_n(x,y)\, W(n\Delta t) \\
\Delta h(x,y) &= \sqrt{h_{\sin}^2(x,y) + h_{\cos}^2(x,y)}\,\mathrm{sgn}(h_{\sin}),
\end{aligned}$$

with

$$\mathrm{sgn}(x) = \begin{cases} -1 & : \quad x < 0 \\ 0 & : \quad x = 0 \\ +1 & : \quad x > 0 \end{cases} \qquad (6)$$

The time delay between two consecutive frames amounts to $\Delta t = (1/7.5)\,\mathrm{s}$, and $W(t) = N \exp\left(-(t - t_{1/2})^2/s^2\right)$ denotes a normalised Gaussian window function with $s = 0.4\,t_{1/2}$ and its centre at $t_{1/2}$, i.e. at the half of the measured time interval.

Figure 9 displays the time averaged height of the central extremum of the surface estimated in this way from the series of measurements at five different temperatures. In the interval from $\bar{B} = 0\,\mathrm{mT}$ to around 24 mT one notices again a monotonic decrease of the central height, due to the growth of the meniscus at the container edge. For higher inductions, ferrogel spikes appear which again lead to a steep increase of $\bar{h}$ for all curves.

Also here, we use the maximal inclination of $\bar{h}(B_0)$, which is determined from a spline, as

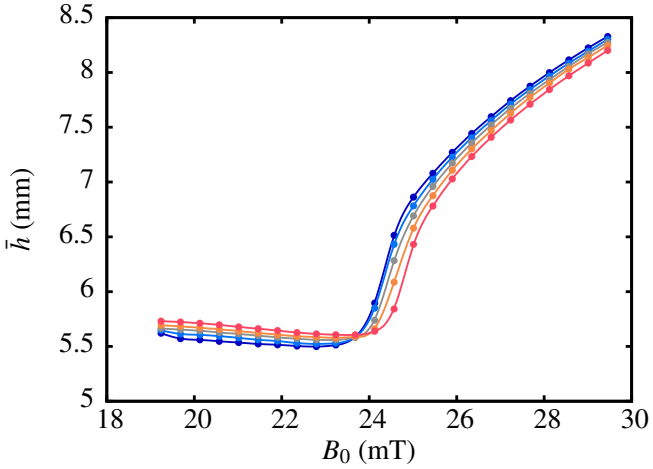

Figure 9: Time averaged height $\bar{h}$ of the central peak of the surface pattern (cf. Fig. 4) versus the bias of the magnetic induction B_0. The lines stem from a spline fit. The colour encodes the temperature as in Fig. 5

an estimate for the threshold. It is denoted by $\tilde{B}_{\mathrm{max.up}}$ and is listed in table 1 for all temperatures investigated. This estimate for the threshold is shifted for higher temperatures towards higher fields. The shift amounts only to $\approx 0.5\,\mathrm{mT}$.

Next, we present the oscillation amplitude Δh of the central spike, as shown in Fig. 10 (a). The amplitude is increasing with increasing temperatures, i.e. for softer ferrogel. From the maximal increase, we determine an additional estimate for the threshold $\Delta\bar{B}_{\mathrm{max.up}}$. The results are listed in table 1. Once more the shift for different temperatures is only $\approx 0.5\,\mathrm{mT}$.

The X-ray movies of our oscillating spikes show, that the response is always harmonic and never sub-harmonic. This is also true for a driven harmonic oscillator. For strong damping and a driving frequency not much smaller than the resonant frequency, the amplitude of an oscillator is inverse proportional to the damping constant. To uncover such a scaling in our measurements, we plot the rescaled amplitude $\Delta h \cdot |\eta^*|$ in Fig. 10 (b), where $|\eta^*| = |G|/\omega$ is the absolute value of the complex viscosity. Within the experimental resolution, the graphs collapse onto a master curve. This indicates that the increase of $\Delta h(B)$ under variation of θ stems solely from the softening of the ferrogel. Therefore, one

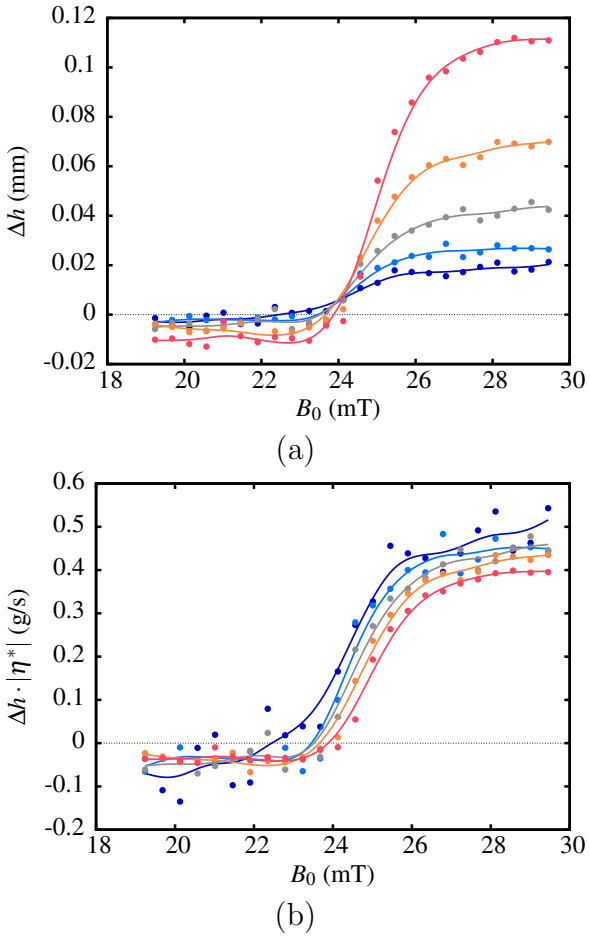

Figure 10: Oscillation amplitude versus the bias of the magnetic induction B_0. (a) Δh of the central peak (cf.Fig. 4) (b) Rescaled amplitude $\Delta h \cdot |\eta^*|$. The lines stem from a spline fit. The colour code for the temperature is the same as in Fig. 5

possible simplified explanation for our experiment could be an oscillator, where the driving force comes from the magnetic stress at the edge of the container and the viscosity provides the damping.

3.3 Comparison of the thresholds with predictions

Now we want to take a closer look at the experimentally determined thresholds of the Rosensweig instability and how they compare to the predictions in Ref. [20]. For a ferrofluid, the threshold can be computed from the nonlinear magnetisation curve, the density ρ and the surface tension σ via the linear stability analysis according to the book by Rosensweig [3], § 7.1. The critical magnetisation M_c of the fluid layer is given by

$$M_c^2 = \frac{2}{\mu_0}\left(1+\frac{1}{r_c}\right)\sqrt{g\rho\sigma}. \qquad (7)$$

Here $r_c = \sqrt{\mu_{ch}\mu_t}/\mu_0$ denotes the geometrical mean of the chord permeability $\mu_{ch} = \frac{B}{H}\big|_{H_c}$ and the tangent permeability $\mu_t = \frac{\partial B}{\partial H}\big|_{H_c}$ at the critical field. Together with $M(H)$ and the jump condition of the magnetic field at the base of the dish, $B = \mu_0\,[H + M(H)]$, the critical induction can be determined from these implicit equations.

For a ferrogel with a Hookean shear modulus G and a linear magnetisation curve, Ref. [20] provides the expression (1). We combine this equation with Eq. (7) for a non-linear $M(H)$ to get the more general form

$$M_c^2 = \frac{2}{\mu_0}\left(1+\frac{1}{r_c}\right)(\sqrt{g\rho\sigma}+G). \qquad (8)$$

If either one of the elasticity or non-linearity is left out, this equation reduces to (1) or (7), respectively.

In table 1, we present the calculated critical inductions B_{cFG} according to Eq. (8). For all calculations, we utilise the storage modulus $G'(1\,\mathrm{Hz})$ as determined by the oscillatory measurements (cf. Fig. 1). The other properties entering Eq. (8) are taken from § 2.2, accordingly. Specifically the surface tension is not well known for our gel. The value used here was $\sigma_{\mathrm{FF}} = 28.7\,\mathrm{mN/m}$. Calculations for $\sigma = 35\,\mathrm{mN/m}$ show that a variation of σ does not change B_{cFG} by more than 5 %. The magnetisation curve has been modeled by the equations given in [34].

The comparison between the experimentally determined thresholds in table 1 and the predictions in Ref. [20] reveals two prominent differences.

Firstly, we observe a decrease of the hysteresis of the pattern amplitude for a decrease of G, i.e. higher temperatures, when the magnetic induction is varied in a quasi-static manner. This hysteresis is denoted in Fig. 11 by the shaded area and the upward and downward oriented full triangles. In contrast, Ref. [20] predicts an increase of the hysteresis under reduction of G for a ferrogel with *Hookean elasticity.*

This can be explained from the temperature dependent relaxation process of the ferrogel. The relaxation times are increasing from $\tau \approx 0.01\,\mathrm{s}$ (at 32 °C) to $\tau \approx 10000\,\mathrm{s}$ (at −10 °C). At the same time the measurement protocol for a full ramping of the magnetic induction was kept at 2 h. The hysteresis increases because the material needs more and more time to follow a variation of B. We have checked that by increasing the cycle time from 2 h to 4 h. The hysteresis was diminished, as shown in Fig. 6.

Secondly, whereas $G'(1\,\mathrm{Hz})$ varies in the investigated temperature range over two decades (cf. Fig. 1), the threshold of the instability is varying only within 10 %. This is in contrast to the model [20] for a ferrogel with *Hookean elasticity.* However we found a different mechanical behaviour of our material. The shear modulus is strongly time-dependent and even vanishes for $t \to \infty$.

In an attempt to select a specific, finite value for G, we modulated the magnetic induction with a fixed amplitude and a frequency of 1 Hz and applied this magnetic driving together with a magnetic bias induction B_0. Under increase of B_0 a threshold is overcome and we observe a steep increase of the time averaged peak height $\bar{h}$. The magnetic induction at which this transition occurs is marked in Fig. 11 by the blue filled circles. Also the oscillation amplitude Δh shows

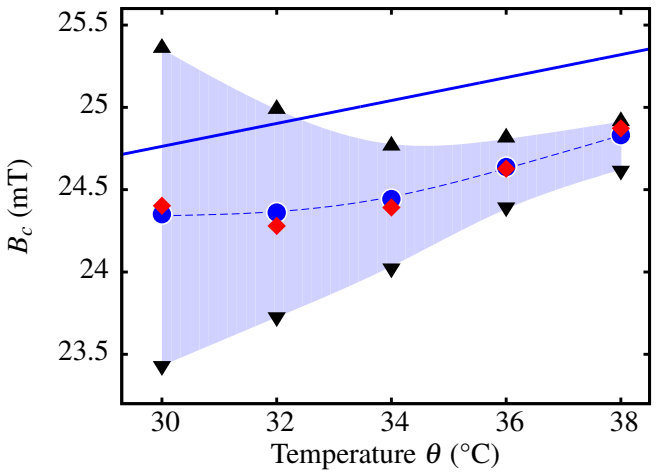

Figure 11: Temperature dependence of the thresholds. The black upward (downward) triangles mark $B_{\mathrm{max.up}}$ ($B_{\mathrm{max.dn}}$) for an adiabatic increase (decrease), respectively. The shaded area in between denotes the hysteresis. The blue circles and red diamonds show $\tilde{B}_{\mathrm{max.up}}$ ($\Delta\tilde{B}_{\mathrm{max.up}}$), respectively. The dashed line is just a guide for the eye. The theoretical value for a ferrofluid is displayed by the solid line.

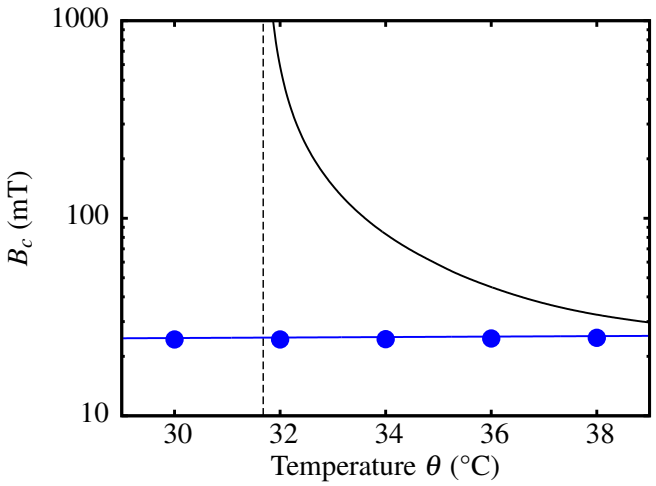

Figure 12: Comparison of theoretically (solid black line) and experimentally (filled circles) determined critical inductions, as listed in table 1. The solid blue line is the theory for a ferrofluid. Note, that in this scale, all experimental values collapse onto that line. The dashed line denotes the vertical asymptote of the theoretical curve at $\theta = 31.7\,^{\circ}\mathrm{C}$.

a steep increase under variation of B_0. The corresponding thresholds are shown in Fig. 11 by red diamonds. Within the experimental scatter both thresholds coincide. Similar to the static experiment, their values vary only in fractions of 1 mT under decrease of the sample temperature θ.

In contrast, the theoretical value, estimated according to (8) at $G'(1\,\mathrm{Hz})$, increases drastically under decrease of θ, as shown in Fig.12. Only for high temperatures, the experimental and theoretical values are close to each other. For lower temperatures, the gap between them increases drastically. According to (8) it even diverges at a critical shear modulus of

$$G_{\mathrm{c}} = \frac{\mu_0}{4} M_{\mathrm{S}}^2 - \sqrt{\rho g_0 \sigma} = 77.8\,\mathrm{Pa}. \qquad (9)$$

For our gel, the saturation magnetisation M_S of the ferrogel amounts to $M_{\mathrm{S}} = 14.7\,\mathrm{kA/m}$ and the divergence occurs at $\theta = 31.7\,^{\circ}\mathrm{C}$. Obviously, there is a mismatch of our complex, soft material and the linear model (8) when implementing $G'(1\,\mathrm{Hz})$.

Let us look more closely on the small variation of the experimentally determined thresholds in Fig. 11. We see that under an increase of the temperature all estimates for the onset of the instability are slightly shifted to higher inductions. This shift can be understood from the fact that for increasing θ the magnetisation diminishes. Utilising the $M(H,\theta)$-model by Ivanov *et al.* [34], we have taken into account this effect. The corresponding results for B_{cFF} are marked in Fig. 11 by the solid line. The good agreement between the experiment and the plain Rosensweig estimate for the threshold computed in this way indicates that the shear modulus $G'(1\,\mathrm{Hz})$ has no influence on the threshold at all.

4 Conclusion

To conclude, we conducted the first measurements of the Rosensweig instability in thermoreversible ferrogels. The present material shows a complex viscoelastic relaxation process with an interesting critical exponent $\beta \approx 1/3$, for experiments carried out in the time domain. It is

possibly explained by a reversible splitting of the polymer network into domains of different size [6,44]. Due to this relaxation, the threshold of the Rosensweig peaks is not much different from the Rosensweig instability in ferrofluids under an adiabatic increase of a static magnetic field. However, the time scales are much slower. This is especially pronounced for the lower part of the investigated temperature range. Experiments with a periodic modulation of the magnetic field show that the *complex viscosity* can be used to describe the response of the ferrogel. Such a complex elastic behaviour, however, is unsuitable to proof or rebut the model of the Rosensweig instability [20], which was derived for just a Hookean shear modulus. Certainly soft matter with finite G for $t \to \infty$ would come closer to that model. One may think that a ferrogel with a higher gelator concentration will serve this aim. However, as a consequence for such a gel, the instability is completely hindered by the strong elastic modulus. Unfortunately, the amount of magnetite cannot be increased further to overcome the critical magnetisation (7). Here, magnetic gels incorporating particles with a higher saturation magnetisation could solve this problem. Despite some attempts, with e.g. cobalt particles, such gels are not yet available.

Acknowledgements

The authors thank H. R. Brand, H. Schmalz, and E.M. Terentjev for helpful discussions and K. Oetter for constructions. We are grateful to Martina Heider for measurements of the surface tension. Financial support by *Deutsche Forschungsgemeinschaft* under the cooperative research project *surface instabilities in ferrogels* within research group FOR 608 (nonlinear dynamics of complex continuous matter) is gratefully acknowledged.

References

[1] B. Berkovski and V. Bashtovoy, *Magnetic fluids and applications handbook*, Begell house, inc., New York, 1. ed., 1996.

[2] ed. S. Odenbach, *Colloidal Magnetic Fluids: Basics, Development and Applications of Ferrofluids*, Vol. 763 of *Lect. Notes Phys.*, Springer, Berlin, Heidelberg, New York, 2009.

[3] R. E. Rosensweig, *Ferrohydrodynamics*, Cambridge University Press, Cambridge, New York, Melbourne, 1985.

[4] Z. Varga, J. Feher, G. Filipcsei, and M. Zrínyi, *Macromol. Symp.*, 2003, **200**, 93.

[5] D. Collin, G. K. Auernhammer, O. Gavat, P. Martinoty, and H. R. Brand, *Macromol. Rapid Commun.*, 2003, **24**, 737–741.

[6] G. Lattermann and M. Krekhova, *Macromol. Rapid Commun.*, 2006, **27**, 1373–1379; *ibid.* 1968 (erratum)

[7] G. Filipcsei, I. Csetneki, A. Szilágyi, and M. Zrínyi, *Adv. Poly. Sci.*, 2007, **206**, 137–189.

[8] K. Zimmermann, V. A. Naletova, I. Zeidis, V. Böhm, and E. Kolev, *J. Phys.: Condens. Matter.*, 2006, **18**, 2973–2984.

[9] M. Babincová, D. Leszczynska, P. Sourivong, P. Čičmanec, and P. Babinec, *J. Magn. Magn. Mater.*, 2001, **225**, 109–112.

[10] L. Lao and R. Ramanujan, *J. Mater. Sc.: Mater. Med.*, 2004, **15**, 1061–1064.

[11] N. J. François, S. Allo, S. E. Jacobo, and M. E. Daraio, *J. Appl. Polym. Sci.*, 2007, **105**, 647–655.

[12] L.-Y. Huang and M.-C. Yang, *J. Magn. Magn. Mater.*, 2007, **310**, 2874–2876.

[13] M. Liu and K. Stierstadt in *Colloidal Magnetic Fluids: Basics, Development and Applications of Ferrofluids*, ed. S. Odenbach, Vol. 763 of *Lect. Notes Phys.;* Springer, Berlin, Heidelberg, New York, 2009; chapter 2, pp. 83–155.

[14] D. Szabo, G. Szeghy, and M. Zrínyi, *Macromolecules*, 1998, **31**, 6541–6548.

[15] Y. L. Raikher and O. V. Stolbov, *J. Magn. Magn. Mater.*, 2005, **289**, 62–65.

[16] C. Gollwitzer, A. Turanov, M. Krekhova, G. Lattermann, I. Rehberg, and R. Richter, *J. Chem. Phys.*, 2008, **128**, 164709.

[17] S. Bohlius, H. Brand, H. Pleiner, and M. Gels, *Z. Phys. Chem*, 2006, **220**, 97–104.

[18] M. D. Cowley and R. E. Rosensweig, *J. Fluid Mech.*, 1967, **30**, 671–688.

[19] V. G. Bashtovoi, *Magnetohydrodynamics*, 1978, **14**(4), 408–410.

[20] S. Bohlius, H. Pleiner, and H. Brand, *J. Phys.: Condens. Matter.*, 2006, **18**, 2671–2684.

[21] A. Gailitis, *J. Fluid Mech.*, 1977, **82**, 401–413.

[22] R. Friedrichs and A. Engel, *Phys. Rev. E*, 2001, **64**, 021406–1–10.

[23] E. Jarkova, H. Pleiner, H. Müller, A. Fink, and H. Brand, *Eur. Phys. J. E*, 2001, **5**, 583–588.

[24] J.-C. Bacri and D. Salin, *J. Phys. Lett. (France)*, 1984, **45**, L559–L564.

[25] J. Browaeys, J.-C. Bacri, C. Flament, S. Neveu, and R. Perzynski, *Eur. Phys. J. B*, 1999, **9**, 335–341.

[26] A. Lange, B. Reimann, and R. Richter, *Phys. Rev. E*, 2000, **61**, 5528–5539.

[27] R. Richter and I. Barashenkov, *Phys. Rev. Lett.*, 2005, **94**, 184503.

[28] J. P. Embs, C. Wagner, K. Knorr, and M. Lücke, *Europhys. Lett.*, 2007, **78**, 44003.

[29] C. Groh, R. Richter, I. Rehberg, and F. Busse, *Physical Review E*, 2007, **76**, 55301.

[30] C. Gollwitzer, G. Matthies, R. Richter, I. Rehberg, and L. Tobiska, *J. Fluid Mech.*, 2007, **571**, 455–474.

[31] R. Richter and A. Lange in *Colloidal Magnetic Fluids: Basics, Development and Applications of Ferrofluids*, ed. S. Odenbach, Vol. 763 of *Lect. Notes Phys.;* Springer, Berlin, Heidelberg, New York, 2009; chapter 2, pp. 157–243.

[32] M. Zrínyi, L. Barsi, and A. Büki, *J. Chem. Phys.*, 1996, **104**, 8750–8756.

[33] M. Krekhova and G. Lattermann, *J. Mater. Chem.*, 2008, **18**, 2842–2848.

[34] A. O. Ivanov and O. B. Kuznetsova, *Phys. Rev. E*, 2001, **64**, 041405.

[35] R. Richter and J. Bläsing, *Rev. Sci. Instrum.*, 2001, **72**, 1729–1733.

[36] A. N. Spyropoulos, A. G. Papathanasiou, and A. G. Boudouvis, Mechanisms of pattern selection in magnetic liquid pools of finite diameter: Realistic computations and experiments, Preprint, 2008.

[37] C. Gollwitzer, A. N. Spyropoulos, A. G. Papathanasiou, A. G. Boudouvis, and R. Richter, The normal field instability under side-wall effects: comparison of experiments and computations submitted, 2008.

[38] R. Kohlrausch, *Pogg. Ann. Phys.*, 1854, **91**, 179–214.

[39] F. W. Kohlrausch, *Pogg. Ann. Phys.*, 1863, **119**, 337–368.

[40] G. Williams and D. C. Watts, *Trans. Faraday Soc.*, 1970, **66**, 80–85.

[41] G. Berry and D. Plazek, *Rheologica Acta*, 1997, **36**, 320–329.

[42] R. S. Anderssen, S. A. Husain, and R. J. Loy, *ANZIAM J.*, 2004, **45**, C800–C816.

[43] A. Hotta, S. Clarke, and E. Terentjev, *Macromolecules*, 2002, **35**(1), 271–277.

[44] S. Baeurle, A. Hotta, and A. Gusev, *Polymer*, 2005, **46**(12), 4344–4354.

The tables should be submitted normally after the reference list, starting on a separate page.

Table 1: Critical inductions for various temperatures: B_{cFF} gives the results of (8) for $G = 0\,\mathrm{Pa}$, i.e. for a virtual ferrofluid with otherwise the material parameters of the ferrogel. B_{cFG} (mT) is estimated from G' at 1 Hz and the measured value of σ. Experimentally, the thresholds were determined from the maximal incliniation of $h(B)$, as marked by $B_{\mathrm{max.up}}$ for increasing B and $B_{\mathrm{max.dn}}$ for decreasing B. From the oscillatory measurements we determine the maximal inclination of $\bar{h}(B)$, marked by $\tilde{B}_{\mathrm{max.up}}$, and the maximal inclination of $\Delta h(B)$ abbreviated by $\Delta\tilde{B}_{\mathrm{max.up}}$

θ (°C)	B_{cFF} (mT)	B_{cFG} (mT)	$B_{\mathrm{max.up}}$ (mT)	$B_{\mathrm{max.dn}}$ (mT)	$\tilde{B}_{\mathrm{max.up}}$ (mT)	$\Delta\tilde{B}_{\mathrm{max.up}}$ (mT)
30	24.76	∞	25.36	23.43	24.35	24.40
32	24.90	587.09	24.99	23.73	24.36	24.28
34	25.04	83.17	24.76	24.02	24.44	24.39
36	25.18	32.51	24.81	24.39	24.64	24.63
38	25.32	28.03	24.91	24.62	24.83	24.87

List of Figures